IAC-12-E2.1.4

Mission and System Design of a 3U CubeSat for Passive GTO to LEO Transfer

Charlotte Lücking* Camilla Colombo†
Colin R. McInnes
Advanced Space Concepts Laboratory
Department of Mechanical and Aerospace Engineering
University of Strathclyde, Glasgow, UK

Abstract

This paper defines a mission concept and system design for a 3U CubeSat technology demonstration. The spacecraft carries an inflatable, ejectable balloon that is used to engineer its area-to-mass-ratio. In this way, the effects of aerodynamic drag and solar radiation pressure on the orbit evolution can be exploited in order to passively transfer from a geostationary transfer orbit (GTO) to a low Earth orbit (LEO). This is of importance since with the increasing interest in CubeSat missions, demand for piggy-back launches to LEO is exceeding availability. In order to tap into the many GTO launches an appropriate strategy is therefore needed to transfer CubeSats from the release orbit into a LEO orbit. The strategy proposed here exploits the effects of atmospheric drag and solar radiation pressure to passively decrease the apogee altitude and increase the perigee altitude respectively. This is achieved by deploying a light-weight balloon that increases the area-to-mass-ratio of the spacecraft. After deployment and rigidisation the manœuvre occurs completely passively, allowing a power down of the spacecraft's electronics for the transfer duration to avoid radiation damage from the Van Allen belts. Once the goal orbit is reached the spacecraft can be powered up again and the balloon is ejected to avoid rapid deorbiting. It is shown that the abandoned balloon is removed from orbit within weeks. The paper contains mission design and scenario selection and the system design of the orbital transfer module.

1 Introduction

CubeSats have in the past decade become the leading platform for low cost space-borne experiments. This is due to their modularised structure and easy access to space. Because of their fixed dimensions they can be launched using a standardised deployment system and launcher interface, sharing a launch with a larger spacecraft. The main orbital region of interest for CubeSat operators is low Earth orbit (LEO). With the increasing interest in CubeSat missions, demand for piggy-back launches to LEO is exceeding availability. In order to tap into the many geostationary transfer orbit (GTO) launches a strategy is therefore needed to transfer CubeSats from GTO to LEO. The transfer needs to be passive since CubeSats typically do not have a propulsion subsystem. Instead orbital perturbations can be exploited which require no active manœuvring.

Fleeter *et al.* have suggested in Ref. [1] to circularise from GTO to LEO using aerodynamic drag and a final propulsive manœuvre. In their design a spacecraft would deploy a drag brake to lower the orbit apogee. Once the apogee is at the desired orbital altitude a propulsive perigee raising manœuvre is performed to insert into a circular LEO. The perigee raising manœuvre is necessary, as without it the fi-

*charlucking@gmail.com
†currently at University of Southampton, UK

nal altitude would be too low for normal operations (below 200 km). This is disadvantageous for CubeSats which would otherwise not need a propulsion system. A propulsion system is complex and costly while small satellites tend to be low-cost and simple.

The method used in this paper is a solar radiation pressure augmented passive GTO to LEO transfer, first introduced in Ref. [2]. It exploits the effect of solar radiation pressure to raise the orbit while simultaneously using aerodynamic drag for apogee lowering. Both aerodynamic drag and solar radiation pressure depend on the area-to-mass-ratio of the spacecraft. By artificially increasing this ratio through the deployment of a large gossamer structure these effects can be enhanced. In this paper a mission concept for a 3U CubeSat demonstrating this manœuvre is described. Section 2 briefly explains the basic concept. Next, Sec. 3 deals with the system design of the satellite, in particular the orbit transfer module. The basic orbital dynamics governing the scenario are then explained and the effectiveness of the method is tested in Sec. 4. Finally an end-to-end mission scenario is devised.

The mission is a proposal for the second United Kingdom universal bus experiment (UKube-2). UKube-1 is a 3U CubeSat due to be launched in 2013 carrying experimental payloads from different UK universities and institutions [3]. Similar to UKube-1 the mission proposed in this paper will offer an opportunity to conduct research during the transfer from GTO to LEO, representing an opportunity to investigate the Van Allen radiation belts in-situ.

2 Mission Concept

The primary mission objective is to demonstrate passive GTO to LEO transfer for CubeSats and other small satellites. The secondary mission objective is to study the Van Allen radiation belts in-situ during the waiting time in GTO and the subsequent orbit transfer manœuvre. A GTO waiting time is likely to be necessary as a piggy-back payload has no influence on the GTO ascending node, while the manœuvre can only be performed when the perigee

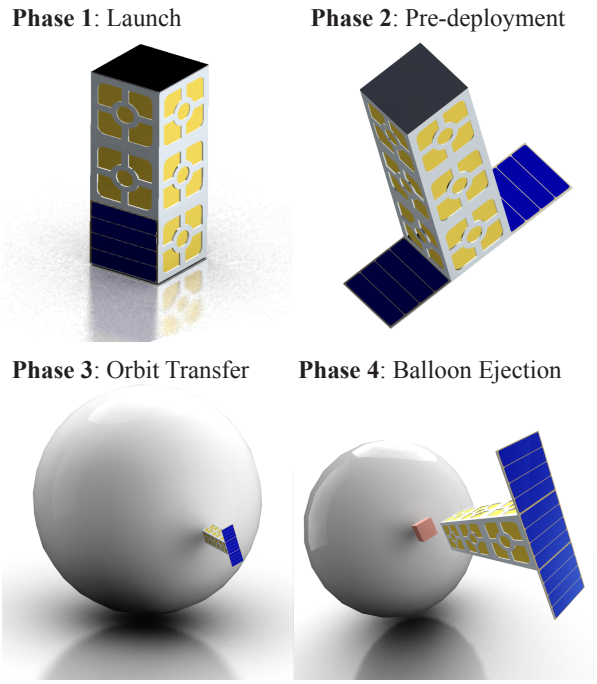

Figure 1: Schematic showing the four configuration phases

vector has a certain direction with respect to the Sun [2]. The governing orbital dynamics will be discussed in more detail in Sec. 4.1.

The mission can be separated into four stages, each of which correspond to a certain hardware configuration (see Fig. 1). During launch the spacecraft is in a stowed configuration to fit within the standard 3U launch container. After insertion into GTO the spacecraft will deploy its solar array panels and wait for the optimum time to deploy the orbit transfer device. After deployment the device will cause the manœuvre to occur passively by exploiting solar radiation pressure and aerodynamic drag. Finally, when the desired LEO is reached the orbit transfer device is ejected to avoid rapid deorbiting.

3 System Design

In this section the design of the CubeSat orbital transfer manœuvre module is discussed. The requirements for the module are defined and then the main design choices are explained and the final design introduced.

3.1 CubeSat Design

The CubeSat consists of three 1U modules, each a standardised 10 cm cube. The total system has a mass of 4 kg which is the standard for 3U CubeSats. The different units are: the orbit transfer module (OTM), the payload module (PLM) and the service module (SVM) (see Fig. 2).

The service module provides power, telecommunications, computing and attitude control services to the spacecraft. Three axis attitude control is necessary in this OTM design, as the inflatable structure needs to be heated using solar radiation prior to deployment as discussed in Sec. 3.4. Since the transfer is completely passive after the deployment, the attitude control is not further needed for the primary mission objective of demonstrating the passive GTO-to-LEO manœuvre. The spacecraft could be powered down for most of the time before reaching LEO to avoid radiation damage. However, to fulfil the secondary mission objective of investigating the radiation belts, continuous attitude control during the orbit transfer is required as the spacecraft needs to avoid being shadowed by the deployed orbit transfer device. The three-axis control can be achieved by using micro reaction wheels in the service module as demonstrated in orbit by BEESAT-1 [4]. For attitude estimation the flux on the solar panels can be used as the spacecraft needs to be Sun-pointing. For power generation the spacecraft is clad on five sides in solar panels. An additional two deployable panels can fold out from the SVM to provide power for the payload instruments. Assuming an attitude in which the deployable device is directed away from the Sun the spacecraft can provide around 6 W of energy.

The payload module is assumed to contain scientific instruments developed by UK universities and institution for the study of the Van Allen radiation belts. The module is left undefined at this stage of the design process.

The orbit transfer module contains a deployable device for enhancing the spacecraft's area-to-mass-ratio to increase the effect of solar radiation pressure and aerodynamic drag. The device needs to be stowed completely within the OTM during launch and the waiting time in GTO. After deployment the device needs to rigidise to ensure the survival against micro-meteorite and debris impacts during the transfer. The device also needs to be ejectable after the transfer is complete to avoid rapid deorbiting. After ejection the device shall deorbit within a short time to avoid collision with other spacecraft. Three main design choices have to be made for the deployable device: which shape should it have, how is it deployed and how is it rigidised and finally ejected. These choices are discussed in the following subsections.

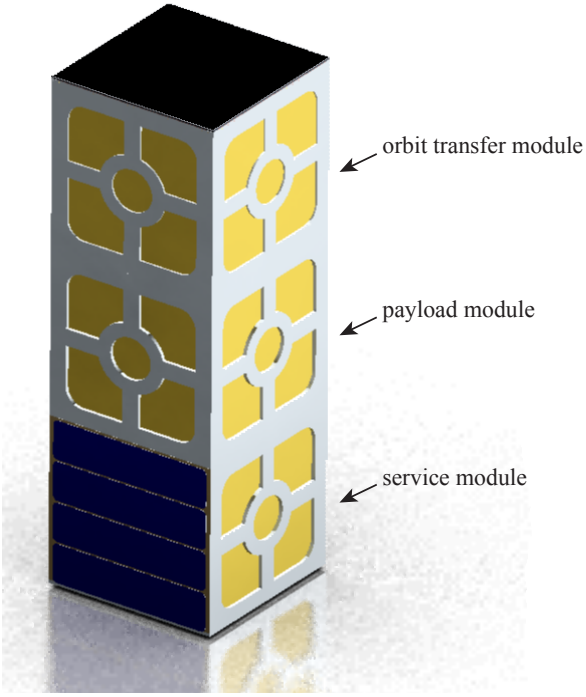

Figure 2: Layout of the CubeSat

3.2 Device Shape

The main options for the shape of the device are a balloon, a cone/pyramid or a flat sail. The cone and the sail need to be directed to face the Sun in order to experience the desired effect on the orbit evolution. Only the balloon is truly passive, however, the balloon would also need eight-times more surface material than the flat sail. This is due to the ratio of surface area of a sphere to its cross-sectional

area and because of the different reflection characteristics of the geometrical shapes.

The coefficient of reflectivity c_R determines the momentum an object gains from incident radiation. It is dependent on the optical properties of the surface material and on the geometrical shape of the object. It is assumed that the material is not transmissive. The incoming solar radiation is partly absorbed and partly reflected. The reflection is part specular and part diffuse. Specular reflection is directional and leaves the surface at an angle which depends on the angle of incidence of the radiation. Diffuse reflection is multi-directional. In this discussion both reflections are considered together as a reflectivity $\eta \in [0, 1]$. While a fully specular reflection without absorption would result in $\eta = 1$, diffuse reflection has a lower reflectivity and is thus approximated as specular reflection plus absorption. This approximation is valid as the material is assumed to be highly specular or mirror-like.

The coefficient of reflectivity of any sphere is one. This can be proven geometrically. First the impulse transmitted to a non-transmissive surface which is tilted by angle $\gamma \in [0, \frac{\pi}{2}]$ with respect to the radiation normal is determined. The incoming radiation is partly absorbed and partly reflected at an angle of 2γ. Figure 3a shows the geometry of this problem. It can be seen that the total impulse along the direction of the incoming radiation is proportional to $1+\eta\cos 2\gamma$. The other part of the resulting force lies in the plane normal to the incoming radiation. This force can be neglected as it will be cancelled out in an axisymmetric shape. Next, the local coefficient of reflectivity can be defined as a function of the in-plane radius from the centre of pressure on the sphere. Figure 3b shows that for a sphere of radius 1 the tilting angle $\gamma = \arcsin r$. Therefore, the local coefficient of reflectivity is $1 + \eta\cos(2\arcsin r)$. This can be integrated to find the total resulting coefficient of reflectivity $c_{R,\text{sphere}}$. The term for the local c_R is multiplied by the circumference at that position and integrated over $r \in [0, 1]$. The integral is then divided by the full cross-sectional area. The resulting value is not dependent on η and always equals one:

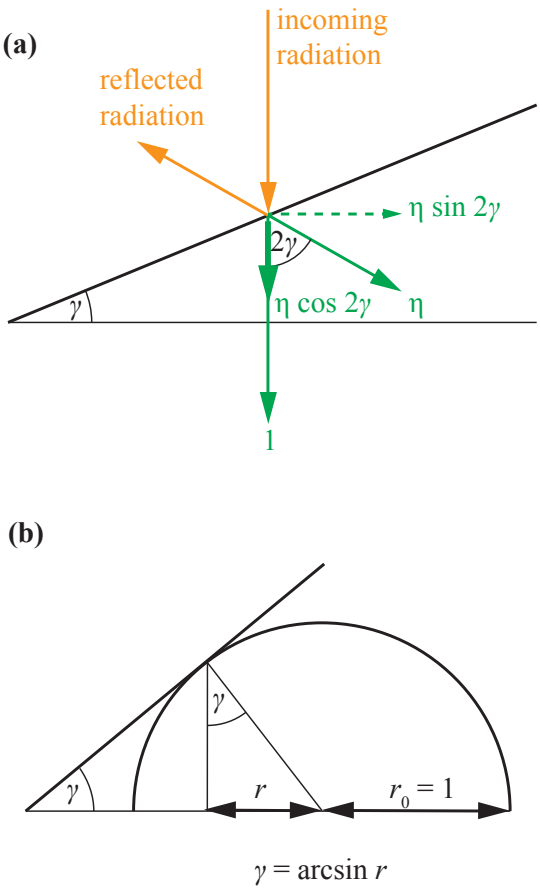

Figure 3: (a) Effective reflectivity of an inclined surface, (b) surface inclination of a sphere

$$c_{R,\text{sphere}} = \frac{1}{\pi}\int_0^1 2\pi r\,(1+\eta\cos(2\arcsin r))\,\mathrm{d}r \qquad (1)$$
$$= 1$$

In the case of a cone or pyramid the tilt angle determines the coefficient of reflectivity as shown in Fig. 3a. For the sphere the orthogonal forces cancel each other out, and for a symmetrical cone or pyramid when the main axis is parallel to the direction of the radiation. The effective coefficient of reflectivity can be written as:

$$c_{R,\text{cone}} = 1 + \eta\cos 2\gamma \qquad (2)$$

It is interesting to note that $c_{R,\text{cone}} = 1$ for $\gamma = \frac{\pi}{4}$, while $1 \leq c_{R,\text{cone}} \leq 1 + \eta$ for $\gamma < \frac{\pi}{4}$ and $1 - \eta \leq c_{R,\text{cone}} \leq 1$ for $\gamma > \frac{\pi}{4}$. The cone or pyramid is a flat sail if $\gamma = 0$. In that case the coefficient of reflectivity is $c_{R,\text{flat}} = 1 + \eta$.

To summarise, while a fully reflective, flat sail oriented normal to the incident sunlight will have an effective coefficient of reflectivity of 2, a sphere will only have an effective coefficient of reflectivity of 1 and thus needs double the cross-sectional area. The advantage of a sphere is that it has the same cross-sectional area from any aspect angle. Thus, after deployment and rigidisation no further control is needed until the device is ejected. The manœuvre will therefore occur completely passively. A flat sail would need to be controlled in order to constantly face the Sun, similar to solar sailing. However, a simpler control algorithm can be implemented because no orbit propagation needs to be performed on-board and the only condition is to keep the sail Sun-pointing. Another advantage over conventional solar sailing is that fast attitude changes do not need to be performed.

A cone or pyramid is a compromise between the balloon and the sail. It requires a medium amount of surface material and due to its conic shape experiences a shuttlecock effect which creates an oscillation around its equilibrium attitude. A cone design would need a mechanism to dampen this oscillation. Then, a constantly Sun-pointing attitude could be assured for altitudes outside the region where aerodynamic drag could be felt. A problem for the sail and the cone also arises when the spacecraft enters the drag region. In this region the force of drag and the force of SRP can act from different directions. The cone would naturally face the direction of the combined force vector.

For this specific mission a sail could be used for the transfer as the secondary mission objective demands an actively controlled Sun-pointing attitude as discussed in Sec. 2. However, the primary mission objective is to prove the concept of *passive* GTO to LEO transfer. Therefore, the device needs to be designed in such a way that it could perform the manœuvre without any control after deployment. Therefore, the balloon shape was chosen.

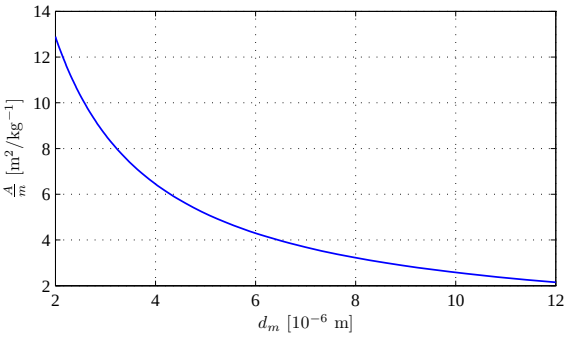

Figure 4: Achievable area-to-mass-ratio of the 3U CubeSat as a function of material thickness for a balloon shaped device

In order to gauge the possible area-to-mass-ratio supplied by a balloon, it was assumed that the surface material of the balloon was Mylar of thickness d_m. The balloon was stowed within 82 % of the volume of a 1U CubeSat module with a packaging efficiency of 50 %. This packaging efficiency was taken from physical tests at the University of Strathclyde [5]. The resulting area-to-mass-ratio as a function of material thickness can be seen in Fig. 4. State-of-the-art solar sail concepts use 2 µm thick Mylar [6], while 12 µm thick metallised PET rescue foil is easily commercially available. It is assumed that a material with a final thickness of 8 µm is plausible. Therefore, an area-to-mass-ratio of $3\,\text{m}^2\,\text{kg}^{-1}$ of the whole system is used. Although the stowed balloon takes up 82 % of a 1U module it weighs less than 200 g.

3.3 Inflation

Possible options for deployment include mechanical methods and gas-based inflation. Mechanical methods extend strut elements using tensile forces by exploiting material properties or using micro-motors. They are not well suited for curved shapes such as a sphere. Inflation is the preferred method for the deployment of spherical shapes as the internal pressure can ensure an even deployment. The gas for the deployment can either be stored in compressed form or be generated in a cold gas generator. The former option is disadvantageous as the gas would need to be stored for a significant time without leaking,

while pressurised containers can be a hazard during launch.

Therefore, a nitrogen gas generator is selected for inflation of the balloon. This mechanism satisfies the key drivers since it can be manufactured cheaply, is very reliable and mass and volume efficient. For 0.5 g of nitrogen one micro gas generator is required which measures 15 cm^3 and weighs of order 8 g [7]. An inflation pressure of 1 Pa is assumed which leads to one generator per 43.5 m^3 of balloon volume using the ideal gas equation and assuming the nitrogen is at room temperature at inflation. This means that with a volume of order 31 m^3 only one generator is needed for inflation.

3.4 Rigidisation and Ejection

Several alternative methods of rigidisation exist. Mechanical rigidisation was used by the Echo balloons, where an aluminium coating on the balloon surface is stretched beyond its yield point through inflation [8]. The advantage of this method is that it works regardless of storage time and under most environmental conditions. The disadvantage is the high mass it requires for the aluminium coating and the extra gas for high internal pressure. This disqualifies the method for use in the OTM device.

Low mass methods of rigidisation use resin with which the surface material is impregnated and which hardens under given circumstances. A popular method is UV curing resin, which hardens when exposed to ultraviolet radiation [8]. This method, however, has a short shelf-life and is thus not applicable for this mission in which a long waiting time in GTO comes before inflation. Other resins will harden when they either heat up or cool down. The former is an irreversible chemical process which cannot be tested before launch. A cold curing resin is the best option. These resin are typically elestomers which harden when they cool below their glass transition temperature [9]. This is advantageous as the balloon will cool down passively after deployment due to its reflective surface material and low mass.

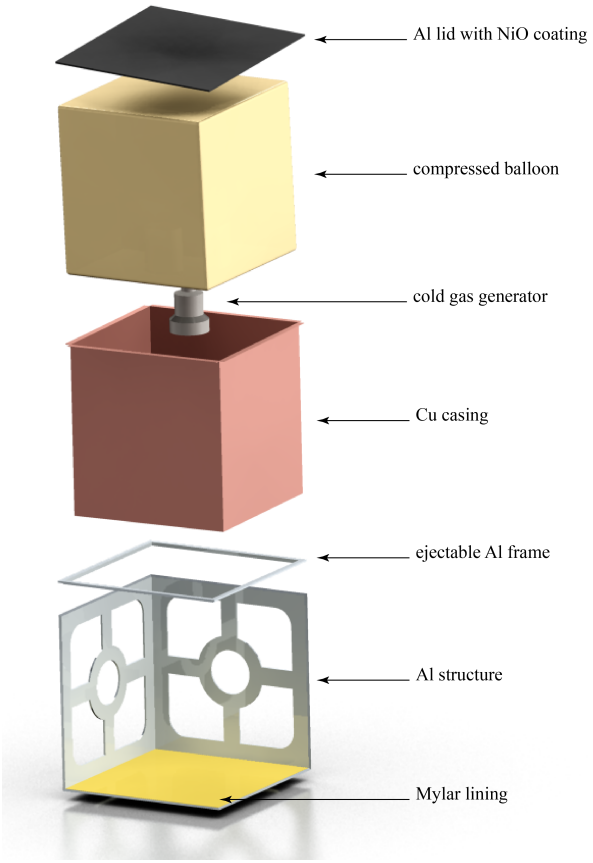

Figure 5: Exploded view of the orbit transfer module

In order to be able to inflate the balloon, it needs to be heated up prior to deployment using solar radiation. This is achieved by turning the spacecraft to face the Sun with the orbit transfer module. The lid of the OTM is coated with Nickel Oxide. NiO has a large solar absorptivity and a low infrared emissivity ($\alpha_{\text{solar}} = 0.9$, $\epsilon_{\text{IR}} = 0.1$), and so will quickly heat up in the Sun. The heat is then transported via a copper casing around the stowed balloon. Copper has excellent heat conduction. To minimise the radiative heat transfer to the rest of the spacecraft, the structure is lined with Mylar which has a very low infrared absorptivity of only 0.03. Figure 5 shows an exploded view of the orbit transfer module.

A transient thermal analysis was performed to determine the required time for the pre-deployment heating process. The lid, the copper casing, the Mylar lining and the stowed balloon were partitioned

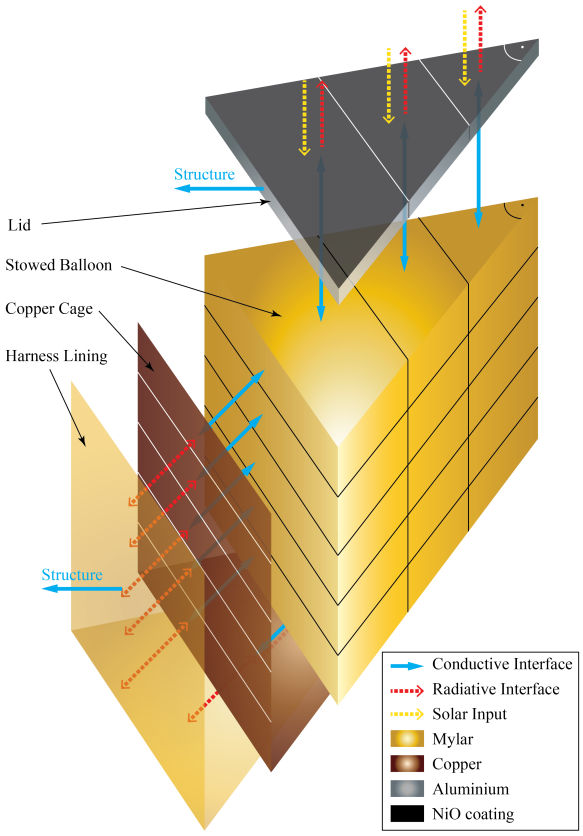

Figure 6: Thermal model of the pre-deployment heating process

into nodes. The differential equations defining conductive and radiative heat exchanges between different nodes were defined as well as the solar radiation input and infrared output. The set-up is visualised in Fig. 6.

These equations were then integrated using the ordinary differential equation solver ODE45 in MATLAB with an initial temperature of 0 °C. The results are shown in Fig. 7. It can be seen that after approximately three hours the whole balloon is predicted to be at a temperature above 60 °C. At this temperature the resin is very soft and pliable and the system is ready for inflation. Tensioned wires holding the lid to the module are cut using pyrocutters and the balloon is forced out of the smooth casing through the pressure of the inflation gas. Importantly, the lid remains attached to the far side of the balloon to avoid becoming space debris.

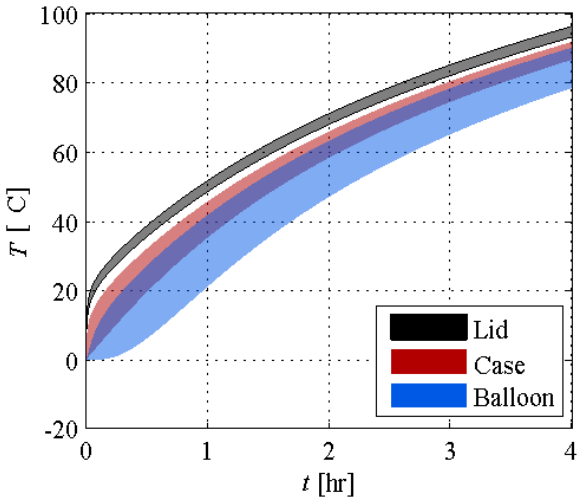

Figure 7: Temperatures during the pre-deployment heating process

The temperatures after inflation were analysed to ensure that the device fully rigidises. To achieve this a worst case scenario was implemented in which the balloon's attitude is fixed with respect to the Sun and the thermal gradient highest. The balloon was assumed to be reflective Mylar on the outside and coated in nickel oxide on the inside to maximise the radiative heat exchange between the Sun facing hot and the cold side. The scenario was computed using the ESATAN thermal modelling suite. The results are shown in Fig. 8 where it can be seen that even in the worst case the maximum temperature is at −20 °C, cold enough for full rigidisation.

Upon reaching the final LEO another tension wire is cut which holds the frame and copper case to the spacecraft. The aerodynamic forces immediately separate the balloon from the spacecraft and the unit deorbits within 9 hr as can be seen in Fig. 9.

4 Mission Analysis

In this section the orbital dynamics of the passive GTO to LEO transfer are discussed in greater detail. Then, a mission scenario is designed using an arbitrarily chosen launch date. Finally, a radiation analysis for the manœuvre is performed and the consequences for the satellite design are discussed.

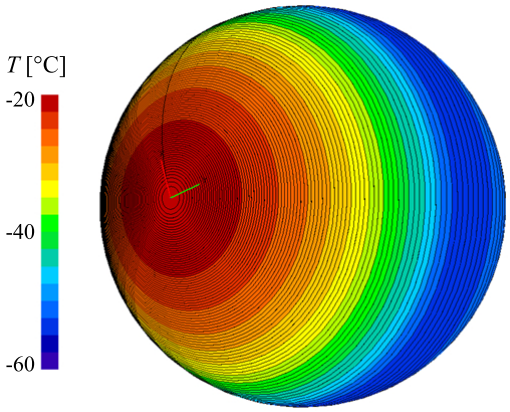

Figure 8: Steady state temperatures of the inflated balloon

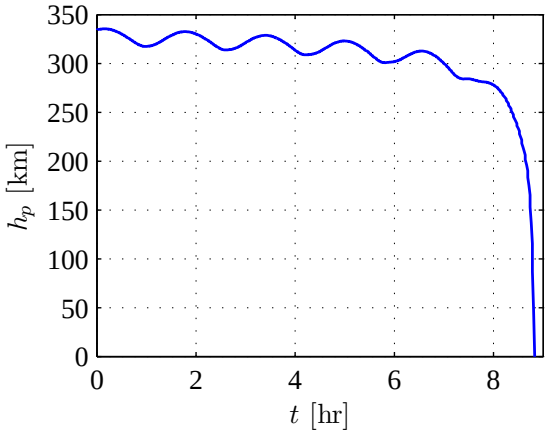

Figure 9: Perigee altitude h_p of the balloon over time after ejection

4.1 Orbital Dynamics

The orbit of a high area-to-mass-ratio spacecraft perturbed by solar radiation pressure will either experience an increase or a decrease in eccentricity depending on ϕ, the angle between its perigee and the direction of the Sunlight [10], where ϕ is defined as:

$$\phi = \omega + \Omega - \lambda_\odot + \pi \tag{3}$$

with ω the argument of perigee, Ω the right ascension of the ascending nodes and $\lambda_\odot$ the right ascension of the position of the Sun on the ecliptic. Figure 10 shows the angles for planar orbits. Planar orbits are assumed to be zero inclination orbits when the tilt of the Earth's axis is neglected.

In the planar geometry the evolution of orbital elements due to solar radiation pressure and the J_2 effect can be analysed analytically [11, 12]. It can be seen that for $-\pi < \phi < 0$ the average change of eccentricity over one orbit is always positive and for $0 < \phi < \pi$ it is negative [13]. The change in ϕ depends on the orbit and the area-to-mass-ratio of the spacecraft. Without the effect of solar radiation pressure and the Earth's oblateness ϕ will always have an average rate of change of $\frac{\mathrm{d}\phi}{\mathrm{d}\lambda_\odot}_{\mathrm{rot}} = -1$ due to the Earth's rotation around the Sun. The average rate of change of ϕ due to the J_2 effect is always positive and dependent on the semi-major axis. For GTO the rate of change due to J_2 is $0 < \frac{\mathrm{d}\phi}{\mathrm{d}\lambda_\odot}_{J_2} < 1$. Therefore the total rate of change $\frac{\mathrm{d}\phi}{\mathrm{d}\lambda_\odot} = \frac{\mathrm{d}\phi}{\mathrm{d}\lambda_\odot}_{\mathrm{rot}} + \frac{\mathrm{d}\phi}{\mathrm{d}\lambda_\odot}_{J_2}$ is negative and $\left|\frac{\mathrm{d}\phi}{\mathrm{d}\lambda_\odot}\right| < 1$, so that one full rotation of the Sun-perigee angle takes more than a year. The effect of solar radiation pressure on the average rate of change depends mainly on the semi-major axis and area-to-mass-ratio. Its sign however is dependent on ϕ. For $-\frac{\pi}{2} \leq \phi \leq \frac{\pi}{2}$ it is positive, else negative.

It can be seen that the value of ϕ at the deployment of the balloon has a significant effect on the success of the manœuvre. For one, the transfer needs to be initiated when $0 < \phi < \pi$, so that the eccentricity decreases and the perigee is raised. Secondly, the manœuvre needs to be performed in such a way that the perigee is within the drag region enough to lower the apogee sufficiently. Therefore, a sharp increase in perigee altitude is not desirable. An analysis of different starting conditions was performed by Colombo *et al.* in Ref. [2], which shows the achievable perigee altitude as a function of the initial Sun-perigee angle, ϕ_0 and the area-to-mass-ratio for GTOs with perigee altitude $h_p = 250\,\mathrm{km}$. The simulation was performed using an analytical approximation of the secular variation of the orbital elements due to solar radiation pressure, the J_2 effect and aerodynamic drag in a planar 2D model [14].It was shown that the GTO to LEO transfer works best for $0 < \phi_0 < \frac{\pi}{4}$.

It is common for spacecraft to be launched into a midnight GTO. In this case the final insertion burn

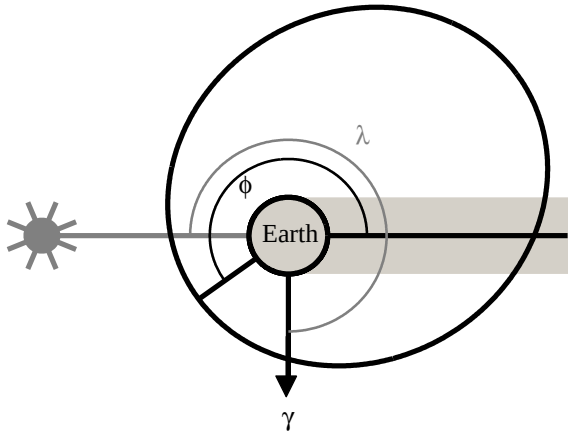

Figure 10: Orbit geometry.

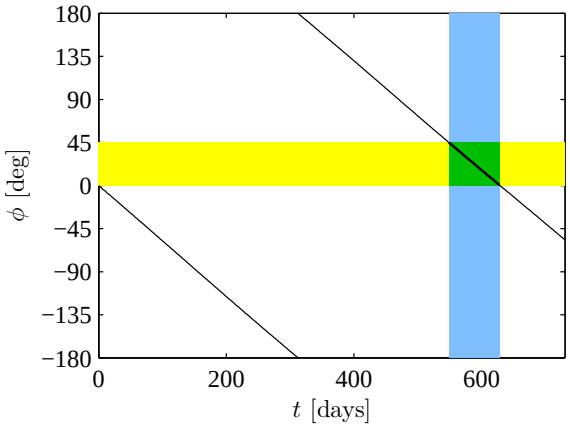

Figure 11: Evolution of the Sun-perigee angle of the GTO after launch

will be performed at midnight which means that perigee is on the opposite side of the Earth from the Sun, *i.e.* $\phi = 0$. This is disadvantageous for the GTO to LEO transfer because for it to be successful ϕ needs to be between 0° and 45°, while the change in ϕ is negative as shown before. Consequently, the spacecraft must remain waiting in GTO for almost a full rotation of ϕ which takes approximately 620 days. Although occasionally GTO launches have different initial orientations towards the Sun, the midnight launch is the most common and also a worst case scenario for the GTO to LEO transfer. Therefore this is the type of launch assumed in this paper. In the next subsection an example mission scenario is defined for an arbitrarily selected launch date of the 1st of October 2014.

4.2 Mission Scenario

The mission analysis is performed using two different orbit propagators. Analytical Graphics Inc. Satellite Tool Kit (STK) is used for high precision orbit propagation (HPOP) including an extensive set of orbital perturbations. Apart from aerodynamic drag, solar radiation pressure and the J_2 effect, HPOP considers the gravitational effects of the Moon and the Sun, the Earth's other gravitational harmonics up to the 21st order and thermal radiation effects. The propagation using this algorithm has a high fidelity but also a high computational time. It is used for the determination of the evolution of single scenarios. For the analysis of a large range of scenarios a MATLAB function is utilised which uses the analytical equations for the secular variations of the 2D planar orbital elements under the effect of SRP, J_2 and aerodynamic drag [14]. This method of propagation is less accurate than STK but can be performed faster.

Three steps are needed for the mission design. After choosing a launch date, the GTO is propagated in STK to get the initial conditions for $0 < \phi_0 < \frac{\pi}{4}$. This is because luni-solar perturbations are assumed to have a significant effect on the orbit during the waiting time causing its perigee altitude to librate. In this propagation a 3U CubeSat is assumed with an area-to-mass-ratio of $0.01\,\mathrm{m^2\,kg^{-1}}$, a drag coefficient of 2.2 and a coefficient of reflectivity of 1.5. From the results of this simulation a table of starting conditions for the orbit transfer is extracted. These conditions are then imported into MATLAB and the 2D propagation is used to calculate the resulting final perigee altitude as a function of waiting time. From this, the best waiting time is chosen and the end-to-end scenario is run in STK. After the balloon ejection, the simulation is run for another year to ensure the spacecraft can maintain its operational orbit for such a period of time.

Figure 11 shows the progression ϕ from GTO insertion. The evolution is steady and it can be seen that after 540 to 620 days of waiting ϕ will be in the appropriate zone for the manœuvre. In Fig. 12 the

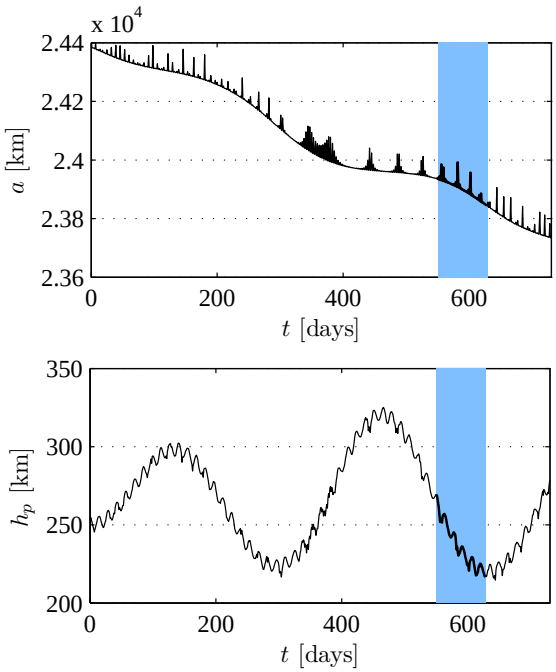

Figure 12: Evolution of the semi-major axis and perigee altitude of the GTO after launch

evolution of the semi-major axis, a, and the altitude of the perigee, h_p are shown. It can be seen that the orbit loses some energy during the waiting time due to aerodynamic drag causing the semi-major axis to decrease. The eccentricity and consequently the perigee altitude oscillate due to third body gravitational effects. This means that at the time of the start of the manœuvre the altitude of the perigee is different than at GTO insertion and measures between 220 km and 270 km.

The different initial parameters for the manœuvre were then propagated in MATLAB to find an approximation of the final perigee altitude after the orbit transfer with a $3\,\mathrm{m^2\,kg^{-1}}$ spacecraft. For this, the orbital parameters of the GTO after different waiting times were propagated until the eccentricity was lower than 0.05 and the orbit thus quasi-circular. The results of this analysis are shown in Fig. 13. It can be seen that the final perigee is higher than the initial perigee for waiting times between 575 and 600 days. As a trade-off between trying to maximise the final perigee altitude and choosing a time in the middle of the interval, a waiting time of 585 days was chosen.

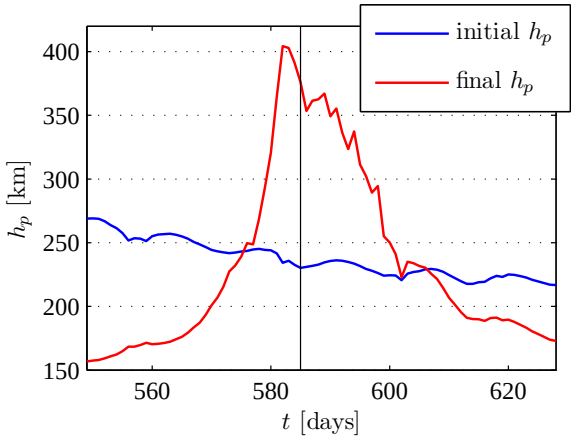

Figure 13: Initial perigee altitude and approximation of the final perigee altitude as a function of waiting time

Finally, the full manœuvre was simulated in STK. The initial parameters were those of a midnight launch GTO from Kourou on the 1st of October 2014. The initial semi-major axis was 24 474 km and the initial perigee altitude 250 km. The inclination was 6°, the argument of perigee 178° and $\phi = 0°$. The orbit was propagated with a stowed area-to-mass-ratio of $0.01\,\mathrm{m^2\,kg^{-1}}$ and $c_R = 1.5$ for 585 days. After that time the area-to-mass-ratio was increased to $3\,\mathrm{m^2\,kg^{-1}}$ and c_R was changed to 1 to model the balloon shape as discussed in Sec. 3.2. When the eccentricity reached 0.05 the area-to-mass-ratio and coefficient of reflectivity were changed back to the original values to model the balloon jettisoning and the propagation was continued for another year.

Figure 14 shows the evolution of the semi-major axis and the perigee altitude during the manœuvre. It can be seen that the semi-major axis remains quasi-constant during the waiting time. When the area-to-mass-ratio changes it decreases rapidly. Finally, in LEO the semi-major axis is stable again. The perigee altitude oscillates during the waiting time. When the balloon is deployed effect of solar radiation pressure causes the perigee to rise for a while before it decreases again slightly. At the end of the orbit transfer the perigee is 100 km above where it started.

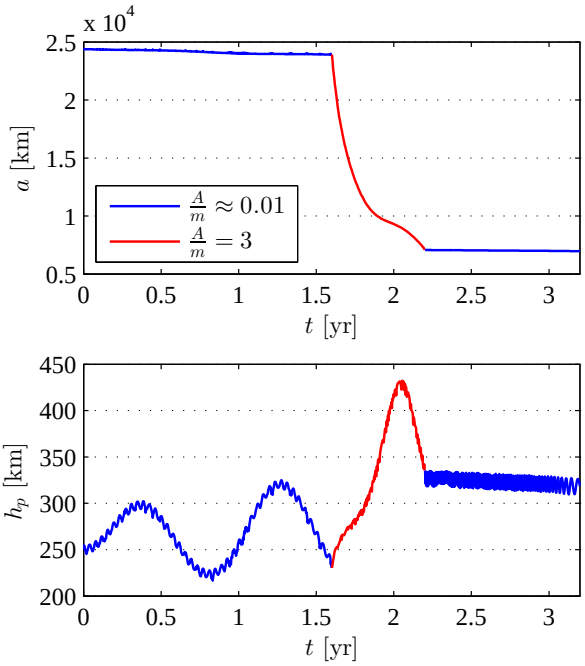

Figure 14: Evolution of the semi-major axis and perigee altitude during the mission.

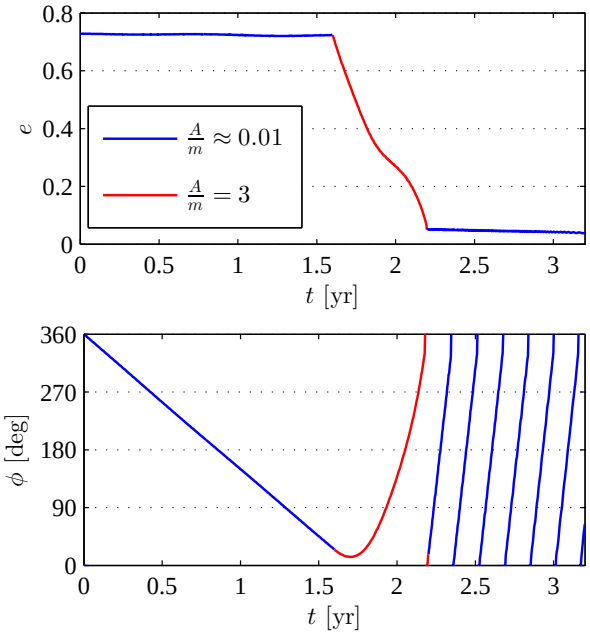

Figure 15: Evolution of the eccentricity and Sun-perigee angle during the mission.

The evolution of the eccentricity and Sun-perigee angle are shown in Fig. 15. It can be seen that whenever the area-to-mass-ratio is low the eccentricity similar to the semi-major axis is relatively stable. It can also be noted that the direction of the progression of ϕ changes when the device is deployed. This is due to the effect of solar radiation pressure on the rate of change of the Sun-perigee angle. In the final LEO the direction of change is still positive even after ejection of the device. This is due to the stronger impact of the J_2 effect on orbits with lower semi-major axis.

4.3 Radiation Analysis

The long waiting time in GTO and the following manœuvre mean that the spacecraft will spend around two years passing through the Van Allen belts. This is an advantage for science missions to study the radiation belts but also a challenge to ensure the satellite survives the harsh radiation environment. As a low-cost mission it is not an option to use expensive rad-hard components. Instead aluminium shielding shall be used to prevent radiation damage. This means that mass will be added to the spacecraft. However, as the orbit transfer system only weighs around 0.5 kg this leaves 3.5 kg for the other two CubeSat units.

A radiation analysis was performed in ESA's space environment information tool (SPENVIS). A file with sampled coordinates throughout the mission lifetime was input into the tool, which then calculated the electron and proton fluxes on the spacecraft. The results are shown in Fig. 16. It can be seen that the fluxes are highest in GTO, during the transfer they decrease and are between two (electrons) and five (protons) magnitudes lower in LEO.

The fluxes were then used to calculate the total ionising dose on a Silicon component as a function of Aluminium shielding thickness d_S. Figure 17 shows the results. It can be seen that while the ionising dose due to trapped electrons decreases almost log-linearly with thickness the ionising dose due to *Bremsstrahlung* and trapped protons stagnates after an initial fast decrease. 7.5 mm spot shielding of sensitive vital components like the flight computer and the flash memory reduces the total ionising dose to 1×10^{-4} rad. According to Wertz and

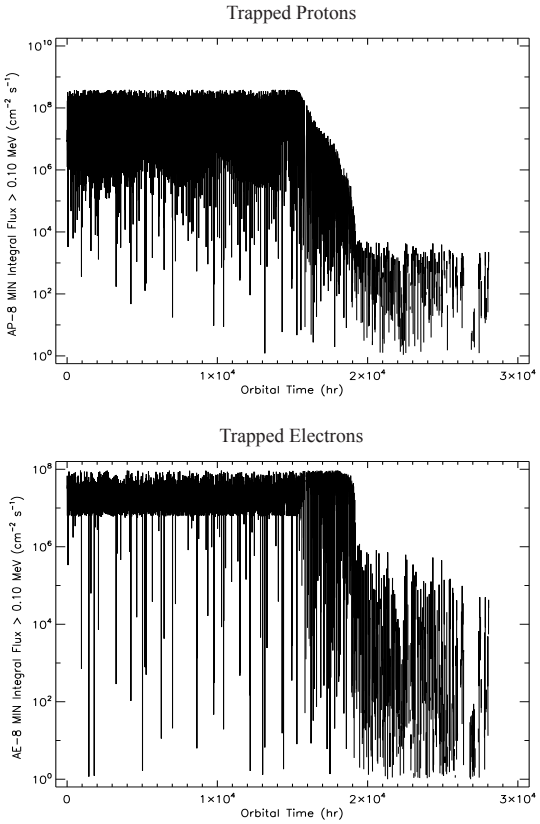

Figure 16: Electron and proton fluxes above 0.1 MeV as a function of mission time.

Larson in Ref. [15] common commercial of the shelf (COTS) components can withstand this amount of radiation.

5 Conclusions

A mission and system design for a 3U CubeSat GTO to LEO transfer has been presented. This is seen as an alternative to LEO piggyback launches. The spacecraft increases its area-to-mass-ratio to use solar radiation pressure and the J_2 effect to simultaneously decrease apogee altitude and raise the perigee to passively reach a LEO orbit without the use of propulsion. The mission scenario was calculated using a high precision orbit propagator and a radiation analysis was performed.

The satellite consists of three 1U modules: a service module, a payload module and an orbit transfer module. The service and payload modules are

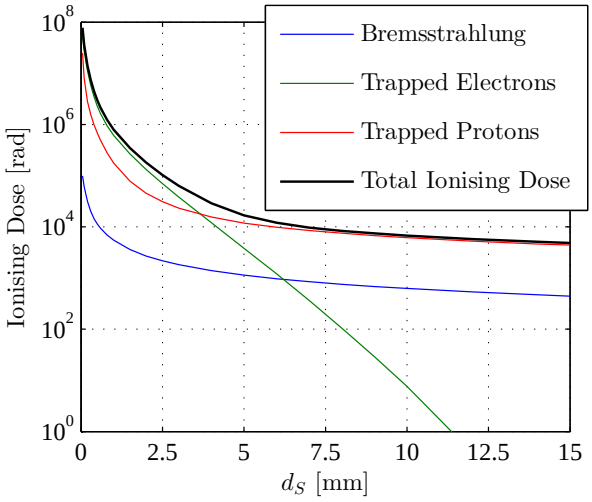

Figure 17: Ionising dose on silicon spacecraft component as a function of the thickness of the aluminium shielding.

aluminium shielded against radiation damage. The orbit transfer module contains a deployable Mylar balloon which when inflated increases the spacecraft area-to-mass-ratio to $3\,\mathrm{m}^2\,\mathrm{kg}^{-1}$. The balloon rigidises after inflation using a cold hardening resin and can be ejected when the final orbit is reached.

The mission presented in this paper offers opportunities to fly payloads in the Van Allen belts to study the radiation environment. It is also a promising low-cost mission concept for a CubeSat technology precursor mission to demonstrate passive orbit transfers using area-to-mass-ratio enhancing technologies. In order to study the radiation belts the spacecraft remains in an operational state throughout the transfer. However, the transfer method and system developed and tested in the mission will also work when the spacecraft is powered down during the manœuvre due to its passive nature.

Acknowledgements

This work was funded by the European Research Council grant 227571 (VISIONSPACE). The educational STK license was kindly supplied by Analytical Graphics, Inc. (AGI). Participation at the International Astronautical Congress 2012 was partly funded by the British Interplanetary Society (BIS).

Charlotte Lücking is also supported by the IET Hudswell Scholarship 2011 and the Frank J. Redd Scholarship.

References

[1] R. Fleeter, D. B. DeBra, P. Gloyer, Z. Wahl, and Goldstein, "Aerobraking Orbit Transfer Vehicle," US Patent No. 6,550,720 B2, 22 April 2003.

[2] C. Colombo and C. R. McInnes, "Propellant-free GTO to LEO transfers," in *Desktop Delta V Workshop*, Providence, RI, USA, 17 February 2011.

[3] C. Clark and S. Greenland, "UKube-1: The first TechDemoCube Multi-payload Nanosatellite." in *20th ESA/CNES 4S Symposium*, Portorož, Slovenia, 5 June 2012.

[4] H. Kayal, F. Baumann, K. Brieß, and S. Montenegro, "BEESAT: A Pico Satellite for the On Orbit Verification of Micro Wheels," in *Proc. of the 3rd International Conference on Recent Advances in Space Technologies*, Istanbul, Turkey, 14-16 June 2007, pp. 497–502.

[5] R. Clark, "Residual Air Inflated System for Passive Deorbiting of CubeSats," MEng Aero-Mechanical Engineering Thesis, University of Strathclyde, 2012, Glasgow, UK.

[6] R. M. Young and C. L. Adams, "TRL assessment of solar sail technology development following the 20 meter system ground demonstrator hardware testing," in *Proc. of the 2nd International Symposium on Solar Sailing*, New York, USA, 20-22 July 2010.

[7] M. C. A. M. Van Der List, L. D. Van Vliet, H. M. Sanders, P. Van Put, and J. W. E. C. Elst, "Applications for solid propellant cool gas generator technology," in *4th International Spacecraft Propulsion Conference*, ser. European Space Agency, (Special Publication) ESA SP. Sardinia, Italy: European Space Agency, 2004, pp. 897–904.

[8] D. P. Cadogan and S. E. Scarborough, "Rigidizable Materials for use in Gossamer Space Inflatable Structures," in *42nd" AIAA/ASME/ASCE/AHS/ASC SDM Conference*, 2001, AIAA-2001-1417.

[9] B. Defoort, V. Peypoudat, M. C. Bernasconi, K. Chuda, and X. Coqueret, *Recent Advances in the Rigidization of Gossamer Structures*, ser. Computational Methods in Applied Sciences. Netherlands: Springer, 2005, vol. 3, pp. 259–283.

[10] C. Colombo, C. Lücking, and C. R. McInnes, "Orbital dynamics of high area-to-mass-ratio spacecraft with J_2 and solar radiation pressure for novel Earth observation and communication services," *Acta Astronautica*, vol. 81, pp. 137–150, 2012, doi: 10.1016/j.actaastro.2012.07.009.

[11] D. P. Hamilton and A. V. Krivov, "Circumplanetary Dust Dynamics: Effects of Solar Gravity, Radiation Pressure, Planetary Oblateness, and Electromagnetism," *Icarus*, vol. 123, no. 2, pp. 503–523, 1996, doi: 10.1006/icar.1996.0175.

[12] A. V. Krivov and J. Getino, "Orbital evolution of high-altitude balloon satellites," *Astronomy and Astrophysics*, vol. 318, pp. 308–314, 1997.

[13] C. Lücking, C. Colombo, and C. R. McInnes, "A Passive Satellite Deorbiting Strategy for Medium Earth Orbits Using Solar Radiation Pressure and the J_2 Effect," *Acta Astronautica*, vol. 77, pp. 197–206, 2012, doi: 10.1016/j.actaastro.2012.03.026.

[14] C. Colombo and C. R. McInnes, "Orbital dynamics of *Smart Dust* devices with solar radiation pressure and drag," *Journal of Guidance, Control and Dynamics*, vol. 34, no. 6, pp. 1613–1631, 2011, doi: 10.2514/1.52140.

[15] J. R. Wertz and W. J. Larson, *Space Mission Analysis and Design*, 3rd ed. El Segundo, Dordrecht: Microcosm Press and Kluwer Academic Publisher, 1999.